Dean&Francis

ISSN 2959-6157

Looking Beyond the Veil: Single Image Dehazing using Untrained Neural Network (SID-UNN)

Ziao Zhou

Tsinglan School, Dongguan, 523808,China;

Abstract:

Haze and fog refer to the suspension of atmospheric particles that significantly diminish visibility, which has always been a concerning issue in our daily lives. Performances of critical computer vision systems are often limited by the hazy weather, posing threats to security and road safety. However, many current dehazing methods rely on complex network or data prior from massive paired datasets which are difficult and costly to obtain, or suffer from artifacts and color distortions. In this paper, I propose a novel dehazing model, SID-UNN, which uses an unsupervised network that requires neither pretraining nor data prior. The model incorporates physical priors in estimating airtight and initializing transmission maps where the parameters are further optimized together with hyperparameters from the network, treating single image dehazing as a nonlinear optimization problem. This unique structure ensures that the estimation does not rely on handcrafted parameters, thus allowing better generalization ability and robustness in the model. Weighted Least Square filtering and smoothing constraints are innovatively applied so that artifacts like halo and noise can be mitigated. Moreover, a benchmarking dataset that includes hazy images in multiple conditions is created. Experiment results on the self-created and synthetic datasets show that SID-UNN has outstanding dehazing ability regarding image details and artefacts that transcend other qualitative and quantitative methods.

Keywords: Dehazing; Image Restoration; Unsupervised Network.

1 Introduction

Haze and fog are serious but common weather phenomena that remarkably diminish visibility even in daylight and exist in many major regions such as Beijing, Sichuan, etc. Reportedly, hazy weather has

become increasingly frequent over the past few decades, with Xi'an having 102 foggy days in 2013 and a visibility of only 2.5 km in the most severe haze event[1]. In addition, the various degradations of images obtained in haze significantly restrict the performance of numerous computer vision systems, including those used in autonomous vehicles, video surveillance, and military applications. Computer vision systems automate various tasks by training computers to identify and utilize image information, such as video surveillance, object detection, and self-driving technologies[2]. However, these tasks demand clear input images that are hard to obtain in the presence of haze. Similarly, an advanced driver-assistance system (ADAS) can use dehazing technology to provide drivers with a real-time picture of the road in hazy weather, reducing the risks of accidents from drivers unable to see the roads ahead[3].

Recent studies on image dehazing mostly follow the physical process of haze formation and employ a widely accepted atmospheric scattering model (ASM) proposed by Koschmieder[4] and McCartney[5], which requires estimating transmission maps and atmospheric light. Popular methods are summarised in Figure 1.

Prior-based methods include DCP[6], haze-lines[7], Atmospheric Illumination Prior (AIPNet)[8], etc. Despite the remarkable performance of these diverse approaches, prior-based methods require handcrafted parameters that rely on experience. Furthermore, they have relatively low generalization capability, leading to incomplete dehazing, colour distortion, or artefacts when facing certain conditions.

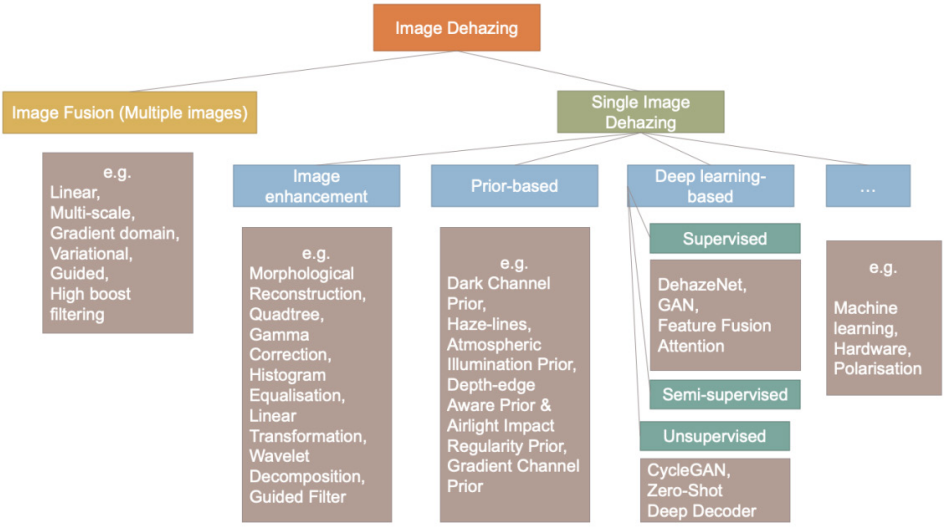

Fig. 1 A categorized summary of common dehazing methods

Supervised methods generally exploit data-driven network models to extract characteristics of input hazy images to compute the haze-free image. Unsupervised deep learning methods treat dehazing as an ill-posed inverse problem, utilizing the natural attributes of the image itself to extract features from the dehazing images to estimate the haze-free image, not demanding a high-standard dataset. For instance, Deep Image Prior (DIP) sets a random initialisation to avoid pretraining but needs a strict regularization[9]. In addition to DIP, deep decoder is a non-convolutional, underparameterised network that does not rely heavily on regularisation and adjusting iteration number, enhancing DIP[10]. However, both of the two technologies are targeted on solving non-linear optimisation problems rather than on image dehazing specifically, revealing problems when directly applying them to dehazing. Zero-shot image dehazing proposed by Li et al. is a network which jointly learn three layers simultaneously – airlight, transmission map, and haze-free image – resulting in being effective but complex[11]. The layered network connotes that a high amount of hyperparameters are required, which puts burden on the convergence of the model.

Specific issues with the existing dehazing methods are identified above, which makes the primary motivation of this research work to solve them. However, trade-offs are involved in addressing these problems, which are complicated to solve with limited resources. Thus, it is hard to surmount all the issues. With this in mind, I propose an improved model, SID-UNN, based on prior works, by which I try to alleviate some of the critical problems in single image dehazing. The model is found to have several highlights:

1. While traditional prior-based methods require handcrafted parameters, my method avoids this parameter dependency and experiences dependency by optimizing the prior parameters with a network.

ISSN 2959-6157

2. Unlike supervised dehazing methods, SID-UNN does not need massive datasets. As a deep learning model based on physical priors, it can effectively handle various scenes and haze conditions with better generalization performance.
3. Compared to unsupervised methods, the proposed model performs the forward generation solely on haze-free images. Parameters of the physical priors are optimized together with network parameters, reducing the model's time complexity and the dehazing network's ill-posedness so that nonlinear fitting can be performed better.
4. Regarding computation speed, initializing the transmission map with a physical prior can ensure a more probable convergence, which is expected to dehaze faster.
5. The quality of the images transcends many methods. Images produced by SID-UNN often have a small halo effect and low noise due to the model's use of WLS filtering and smoothing constraints.
6. A benchmarking real-world dataset uniquely shot in several classified conditions is created.

2 Proposed method

2.1 Atmospheric Scattering Model (ASM)

Koschmieder and McCartney express the optical process of haze formation on captured images as the Atmospheric Scattering Model (ASM), as shown in Figure 2. Light reflected from objects in the scene experiences attenuation as it travels a distance from the scene to the camera. Additionally, the scattering by atmospheric particles introduces airtight to the image. Thus, the model's formula, presented as the following, includes two terms: direct attenuation and airtight. The former determines the colour, and the latter the visibility of the image.

$$I(x)=J(x)\cdot t(x)+A(1-t(x)) \quad (1)$$

In Eq. 1, I is the hazy image, J is the haze-free image, t is the transmission map, A is the global atmospheric light, and x is the pixel coordinates. The transmission map indicates the fraction of light $(t(x)¡\hat{E}[0,1])$ that reaches the camera without being scattered, defined as:

$$t(x)=e^{-\beta d(x)} \quad (2)$$

Where β denotes the scattering coefficient, $d(x)$ symbolizes the depth or distance from the scene to the camera. Eq. 1 makes SID as an ill-posed problem, as two parameters, t, and A, must be estimated from the known I to find J, motivating researchers to develop more accurate calculation methods.

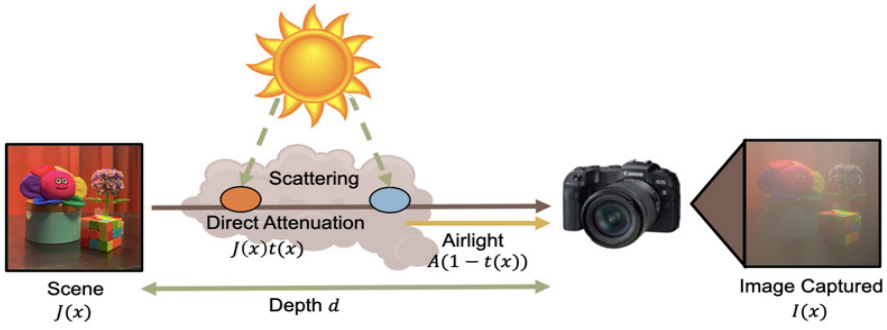

Fig. 2 The atmospheric scattering model

2.2 SID-UNN Model

The proposed dehazing method SID-UNN comprises two estimation stages, as shown in Figure 3. In the first stage, haze-free images are generated by a Convoluted Neural Network (CNN) with a random initial value, simultaneously estimating the two maps needed for ASM. The transmission map is preliminarily estimated with DCP and smoothed using Weighted Least Square (WLS), which exposes two parameters. Atmospheric light is calculated with quadtree decomposition and set as constant. Such designs of using the network to generate only the haze-free map significantly decrease the network's ill-posedness and reduce the overall complexity of the model, thus demanding a less complicated regularisation and ensuring a more robust nonlinear convergence. Furthermore, incorporating the physical prior frees the requirement of data prior, utilising only CNN's nonlinear fitting ability to obtain the best solutions which enhances the computational speed.
Optimization parameters of the transmission map are put into a parameter space along with the hyperparameters of the CNN network used to generate haze-free images. Subsequently, both types of parameters are sent to an optimizer. By adjusting the transmission map parameters through an optimizer, I avoided using handcrafted parameters that rely on empirical priors. Therefore, the model can be ap-

plied to more generalized situations as people do not need to change the image-specific parameters. In the generated haze-free image, a unique smoothing constraint is added to reduce the effect of noise on optimization. In the second phase, a forward physical model is constructed to convert the estimated haze-free image back into the hazy image. The calculated transmission map and atmospheric light are used to build the forward model based on ASM. The loss function is then computed between the input and the generated hazy image, which is then sent back to the optimizer to adjust the targeted parameters, aiming to minimize the loss and improve the model's accuracy. Thus, a model without pre-training and a massive dataset can be achieved.

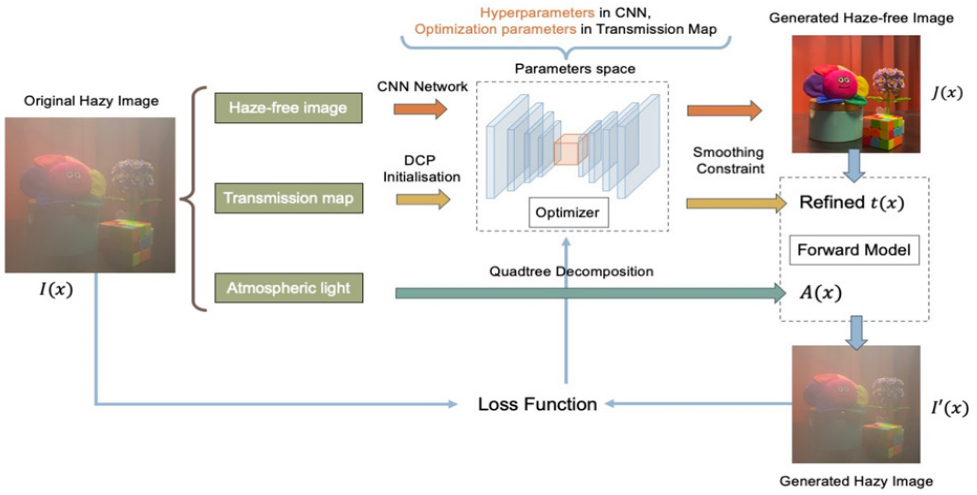

Fig. 3 Framework of SID-UNN

2.3 Physical Prior

2.3.1 Dark Channel Prior with Weighted Least Square Filtering

DCP bases its dehazing mechanism on an empirical observation that for most natural images, pixels in local patches apart from sky regions have at least one colour channel of RGB exhibiting very low intensity. Thus, channels of near-zero intensity, or "dark channel" I^{dark}, are identified by iterating each pixel in the local patch, which is formulated as follows:

$$I^{dark}(x) = \min_{C\in R,G,B}\left(\min_{y\in\Omega(x)}\left(I^{c}(y)\right)\right) \quad (3)$$

$$I^{dark}(x)0(4) \quad (4)$$

Where x is pixel coordinates, Ω is the patch of pixels centred in x, I^c is the colour channel c of R, G, and B from I, and y is the pixel in Ω(x). Subsequently, substituting Eq. 3 into Eq. 1, the ASM, and rearranging to make transmission t(x) as the subject will give:

$$t(x) = 1-\omega \min_{y\in\Omega(x)}\left(\min_{c}\frac{I^{c}(y)}{A^{c}}\right)(5) \quad (5)$$

An aerial perspective parameter ω is given on the minimization term to ensure an authentic look of the generated haze-free image, usually set to 0.95. The transmission map is initialized with the formula Eq. 5. With a pre-estimated transmission map, the model's time complexity is largely reduced, thus decreasing the computation pressure.

To improve the efficiency of the smoothing process, the proposed SID-UNN uses the WLS optimization framework[12], [13], which is more advantageous in reducing halo effects and preserving edges than other common processing methods, such as guided image filtering and bilateral filtering. Furthermore, WLS can migrate small features to the detail layers so that details in the images can be conserved.

WLS optimization seeks a new image that closely resembles the original while maintaining smoothness throughout the image except in areas across significant gradients. The searching process is expressed as the minimum of the following:

$$\sum_{p}\left(\left(u_p-g_p\right)^2+\lambda\left(a_{x,p}(g)\left(\frac{\partial u}{\partial x}\right)_p^2+a_{y,p}(g)\left(\frac{\partial u}{\partial y}\right)_p^2\right)\right) \quad (6)$$

Where p signifies a pixel location, g denotes the input image, and u denotes the new image to be found. a_x and a_y are smoothness weights that depend on g, and λ is a coefficient that controls the balance of the two weights. (Larger λ values create smoother images u.) The following two equations show how the smoothness weights are defined:

ISSN 2959-6157

$$a_{x,p}(g)=\left(\left|\frac{\partial \ell}{\partial x}(p)\right|^{\alpha}+\epsilon\right)^{-1};$$

$$a_{y,p}(g)=\left(\left|\frac{\partial \ell}{\partial y}(p)\right|^{\alpha}+\epsilon\right)^{-1} \quad (7)$$

Where l is the log-luminance channel of the input image g, α indicates the sensitivity to gradients g, while ε is a small constant that prevents a zero denominator in areas where g is constant.

In our model, ε is set to 0.0001, while α and λ have separated values for different haze densities. For thin haze, α is 4 and λ is 0.35; for heavy haze, α is 7 and λ is 0.8.

2.3.2 Quadtree decomposition

Quadtree decomposition is incorporated to calculate the global atmospheric light by extracting the sky region from hazy images, a region with the thickest haze that is considered smooth, bright, and at the top of most natural images. The input image is segmented evenly into four regions. According to the observation that the sky region is often at the top of images, the top right and top left quadrants in each division are chosen to be further divided into four sub-quadrants. Next, the average brightness and the average gradient of each sub-quadrant are computed, expressed as:

$$I_{\phi,i}^{light}=\frac{1}{N_{left,i}}\sum_{n=1}^{N_{left,i}}\left(\frac{1}{3}\sum_{c\in\{r,g,b\}}I^{c}(n)\right);$$

$$I_{\phi,i}^{light}=\frac{1}{N_{\phi,i}}\sum_{n\in\Delta_{\phi,i}}^{N_{left,i}}\left(\frac{1}{3}\sum_{c\in\{r,g,b\}}\frac{\partial\left(I^{c}(n)\right)}{\partial n}\right) \quad (8)$$

N_{left}, i represents the number of pixels in the top left quadrant i, and $I^{c}(n)$ is the nth pixel in the colour channel c ($c\in\{r,g,b\}$). To find the sub-quadrant with the largest brightness and low gradient change as these characteristics are entailed for sky regions, sub-quadrants are selected by solving the following:

$$\arg\max_{i}\left\{I_{\phi,i}^{light}\right\};$$

$$i\in\left\{0,2,3,I_{\phi,i}^{grad}\leqslant\frac{1}{4}\sum_{i=1}^{4}I_{\phi,i}^{grad}\right\} \quad (9)$$

The selected sub-quadrants are divided into four quadrants and calculation of Eq. 8 and Eq. 9 is repeated until an acceptable quadrant is found. The centre pixels of the two found quadrants are set as feature pixels. Regions with similar luminance to the segmented areas where the feature pixels are located are merged to form the sky region. Atmospheric light is then taken as the largest intensity in this sky region.

2.4 Smoothing constraint

An innovative smoothing constraint is added after a haze-free image is generated from the model, achieved through Exponential Moving Average (EMA) expressed as follows.

$$O^{smoothed}(x)=O(x)*\gamma+O'(x)*(1-\gamma) \quad (10)$$

Where O(x) represents the output of the previous iteration, O'(x) is the output of the current iteration, $O^{smoothed}(x)$ is the smoothed image of the current output O'(x), and x is the pixels. Coefficient γ controls the extent of smoothing, with a higher value indicating a smoother image. This variable could be changed manually according to the amount of noise in the original image, but setting it as a constant is often enough to satisfy our intention. In this model, γ is 0.90. This smoothing constraint will enable the final output to maintain good high-frequency details while filtering out noise, making the method more robust and adaptable.

2.5 Loss Function

Loss is calculated between the original hazy image and the generated hazy image after it goes through the forward ASM. L1 loss, also known as Mean Absolute Error (MAE), finds the absolute difference between two values and is one of the popular loss functions for neural networks. Several tests were carried out with L1, L2, and total variation loss as loss functions on SID-UNN. Results connote that L1 loss is most suitable with the proposed model, with L2 loss demonstrating colour shifts and total variation loss unable to converge to a correct image. Therefore, L1 loss is adopted and expressed as follows:

$$L=\frac{1}{N}\sum_{i=1}^{N}I_{original}^{i}-I_{generated}^{i} \quad (11)$$

Where $I_{original}^{i}$ is the input image, and $I_{generated}^{i}$ is the generated hazy image.

2.6 Network Architecture

A U-net hourglass network architecture with skip connections is adopted in this work. The network has two paths: a contracting path of encoder layers responsible for feature extraction and an expansive path of decoder layers capable of decoding the encoded data and utilizing information transferred from the contracting path through skip connections.

In the encoder stage, CNN operations are performed to obtain a feature map of the input image, which is reduced in the spatial dimensions and increased in the depth. Two 3x3 convolutions are conducted in each layer, subsequently operated with a 2x2 max-pooling. Starting with

64, the feature channel of the network doubles along the contracting path and halves along the expansive path, with the bottleneck having 1024 channels. The decoder process restores the abstracted features by increasing the special resolution of the feature map and utilizing information provided from the contracting path. Upsampling is achieved by performing a 2x2 up-convolution followed by two 3x3 convolution layers and a ReLU activation in each level, ending with a 1x1 convolution before the image is reconstructed to the original spatial size at feature channel 2.

Skip connections, the typical characteristic of U-Net, help retain high-resolution features that may be lost during downsampling in the encoder, improving the accuracy and detail in the output image. Feature maps from the contracting path crop concatenate with those in the expansive path of the corresponding level, allowing the preservation of both high-level and low-level features and alleviating omitted gradients.

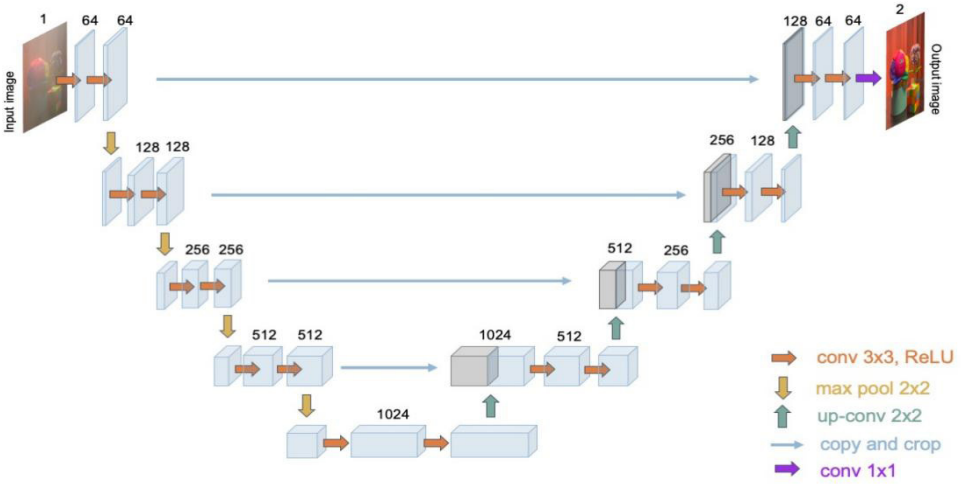

Fig. 4 The hourglass network architecture with skip connections used in SID-UNN comprises the contracting and expansive paths

3 Experiment

3.1 Dataset of synthetic images

Experiments are carried out partially on the REalistic Single Image DEhazing (RESIDE), a recent, large-scale dataset[14]. One of the subsets, the Hybrid Subjective Testing Set (HSTS), comprises 10 synthetic and real-world hazy images, all taken from different scenes. Images are synthesized using a forward ASM physical model with handcrafted parameters, whereas realistic images are taken outdoors.

3.2 Hazing experiment

The self-created dataset, Real-world Multiple-condition Grading Dataset (RMGD), is a single image dehazing benchmark composed entirely of realistic hazy images to ensure better compatibility with the common objective quality evaluation metrics such as PSNR and MSE and enables better juxtaposition in subjective evaluation. The dataset compromises 5 subsets of different degrees of haze – haze-free, light haze, heavy haze, non-homogeneous haze, and light haze in white background, each possessing images of various scenes. There are 49 images, some picturing the same scene but in different haze conditions. In those images of the same scene, all other constants, such as angle of shooting, light intensity, position of objects in the scene, etc., are unchanged. Specifically, the camera is set around 15 degrees above the horizontal to shoot the scene. Two lamps (approximately 500 lumens each) provide enough light to illuminate all details in the scene and reduce the shadow on objects that obscure certain details.

3.2.1 Experimental Design

Hazy images are taken indoors, and the facilities are positioned as displayed in Fig. 5. Haze is imitated by a large fog-producing humidifier, which is placed between the scene and the camera. As most fogs in real-life situations have water vapour as a major component, it can be justified to simulate the outdoor haze with a humidifier. To guarantee the haze is evenly distributed in the image, the camera shoots at the scene from the nozzle spray, where the haze is most concentrated. The camera is fixed on a tripod and maintained at the same place for each subset of

ISSN 2959-6157

scenes to ensure the shooting angle is controlled. Objects in the scene are typically chosen with saturated colours and range from various textures such as glass, plastic, and cloth. Thick and non-homogeneous haze are generally challenging tasks for dehazing: to evaluate the full potential of a dehazing algorithm, more challenging tasks should be given. A whiteboard is behind the scene to generate a white background, or the "sky". Images with "sky" are included because some methods, like DCP, are less capable of dealing with this issue. Additionally, haze-free images allow objective and subjective comparisons of the clear and dazed images.

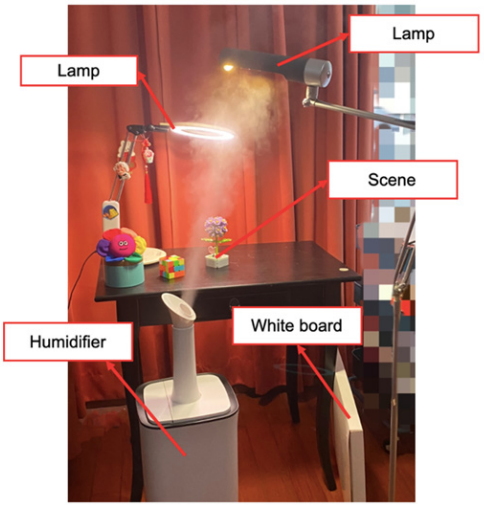

Fig. 5 A labelled diagram of the scene setup, light source, and haze simulator

3.2.2 Benchmarking

The created dataset RMGD is entirely composed of real-world images. While synthetic hazy images often appear unrealistic and dehazing such images appears unnatural, a real-world dataset avoids the domain shift issue. The new dataset provides images under various conditions, some not commonly embodied. For instance, this dataset contains images of a white background, providing a convenience for researchers to test "sky" region issues which establishes a standard on a dehazing method's ability and highlights a certain method's strengths. For example, a method capable of processing non-homogeneous haze may not be displayed when using datasets containing only thin haze, but with this dataset, the method's ability can be directly contrasted with other methods using this same dataset.

4 Results

4.1 Evaluation metrics

Two mainstream metrics are considered in the results: Peak Signal-to-Noise Ratio (PSNR) and Structural Similarity Index (SSIM). A high PSNR value denotes that the generated image is similar to the original haze-free image, with less distortion or noise introduced during the dehazing process. PSNR requires a strict ground truth to conduct its assessment. However, because the self-created dataset is shot in the real world, it is impossible for every pixel's position in the image to be unchanged. SSIM will not be used for images from RMGD.

4.2 Configurations and dehazing speed

Experiments are conducted on two 80-core RTX-A6000 GPUs with 128GB memory. The operating system installed is Ubuntu 18.04 LTS, and Python 3.7 is the coding language. The ADAM optimizer is used, and the learning rate and number of iterations are adjusted to 0.01 and 2600, respectively. Hazy images are all resized to 600x600 before dehazing. In this setting, the speed of computation is around 350 seconds. Although this value is insignificant compared to other mainstream methods, switching to better hardware can improve the speed.

4.3 Experimental results on a synthetic dataset

4.3.1 Qualitative Analysis

Four popular algorithms are compared with SID-UNN: DCP[6], AOD-Net[15], DehazeNet[16], GCANet[16]. From Figure 6, it can be found that SID-UNN is better than all other four methods. AOD-Net suffers from incomplete haze removal, exemplified by a layer of thin haze that still covers the image in all three rows. In the first row, it is evident that both DCP and DehazeNet suffer from excessive exposure, where details of the lights are mixed with the wall, whereas GCANet has blurred between the light and the curtain. SID-UNN provides an image most similar to GT visually in terms of its details. In the third row, colour distortions that lead to a yellowish table are present in almost every method. While GCANet gives a table colour resembling GT, the wall colour appears darker. In contrast, SID-UNN offers a correct wall colour but a more distorted table colour. Similarly, colour distortion is again prevalent in the second row, with many wall colours being overly yellow relative to GT. While AOD-Net and GCANet have the closest wall colour value, some haze remains unremoved in the top right corner. Among the rest of the methods, SID-UNN seems the best.

Fig. 6 Results of SID-UNN and other methods on indoor hazy images. Results of the other methods (b)-(e) are cited from Qin et al.'s work[17]we propose an end-to-end feature fusion at-tention network (FFA-Net**, in which they calculate the images using algorithms from the original authors. This work does not calculate these images directly because of the hardware limitations.**

Moreover, two outdoor hazy images were tested using SID-UNN. The result is less satisfying regarding its ability to dehaze sky regions. Sky regions suffer from over-enhancement, as shown in Figure 7. This is due to the use of DCP as the physical prior, which inherently makes SID-UNN vulnerable to sky dehazing. Apart from the sky regions, the details of the buildings and roads have recovered outstandingly. For example, in the first image the windows of the buildings are reconstructed to almost the same as the GT.

Fig. 7: Outdoor results of SID-UNN.

4.3.2 Quantitative analysis

The performance of SID-UNN and the other methods mentioned above is evaluated using the PSNR metric. As Table 1 shows, the proposed method surpasses the other four methods by a large margin.

Table 1: Quantitative result of SID-UNN and the state-of-the-art methods regarding the images presented above. Data from the four methods are cited by Qin et al.[17]we propose an end-to-end feature fusion at-tention network (FFA-Net, where they calculate the PSNR for each (b)-(e) image in Figure 7.

Methods	DCP	AOD-Net	DehazeNet	GCANet	FFA-Net	SID-UNN
PSNR	16.62	19.06	21.14	30.23	36.39	66.8

ISSN 2959-6157

4.4 Experimental results on RMGD

Figure 8 displays the results of SID-UNN and DCP using inputs under four different conditions. Overall, SID-UNN seems to have similar outputs to DCP regarding colour but outperforms DCP in detail in the generated images.

The first three rows, Fig. 8(i), show images with heavy haze, in which both DCP and the proposed method perform well in generating the correct colour and constructing details. However, if we look closely, results by DCP contain colour patches and abrupt jumps from one patch to another, whereas images generated by SID-UNN appear more natural and smoother, as exemplified by the magnified selected regions in the fourth column. These patches are not the consequences of the low resolution of images, as input images are in 600x600 for both methods; instead, it is because of the innovative smoothing constraint and WLS filtering employed in SID-UNN incorporates, so images look smoother, enhancing the visual quality of the dehazed images.

The middle two rows of Fig. 8(ii) are images with a thin haze. Apart from the differences mentioned above, obvious colour distortions appear in DCP results, as in the colours of the flowers, which look bluer and darker. The proposed method alleviates this over-saturation problem, and visually, the colours of the results by SID-UNN are closer to the real colours of the scene.

A small issue is that SID-UNN cannot completely avoid the over-enhancement problem faced by DCP; the colours of dehazed images still look darker than they should be in GT. Nevertheless, it is unrelated to the proposed model's structure and thinking. This issue is because SID-UNN uses DCP as the initial estimation of the transmission map, relying partially on the accuracy of DCP's estimations. Changing to a better physical prior may solve this issue. For the same reason, SID-UNN's ability to deal with images with white backgrounds and non-homogeneous haze is relatively weak, as shown in Fig. 8(iii)-(iv). Another reason is that the classification of the thickness of haze is not unified; even the thin haze captured in this dataset is often heavier than other synthetic datasets. The thick haze tends to induce over-enhancement issues. Under such considerations of heavier haze, it is good enough for SID-UNN to dehaze to this extent.

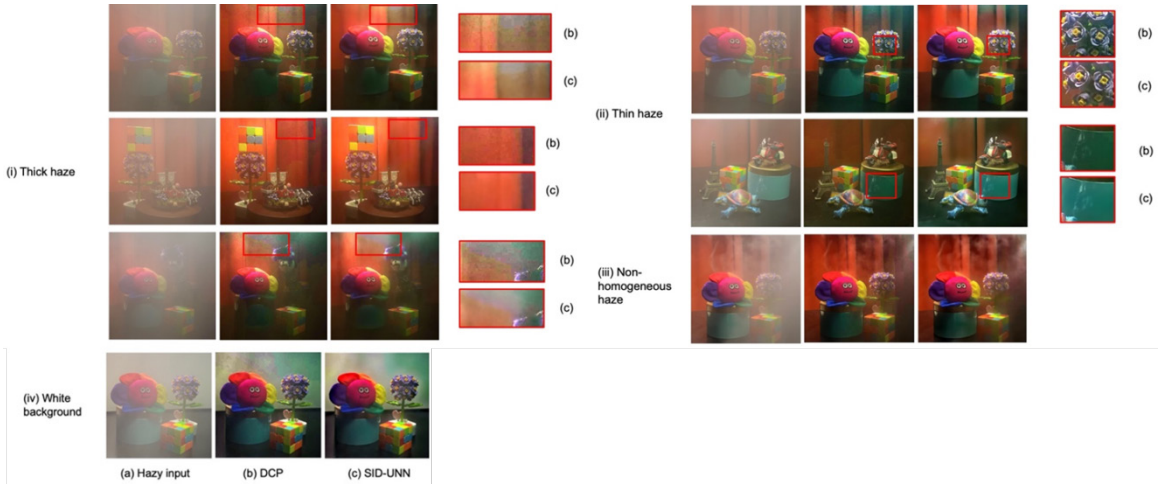

Fig. 8 Results by DCP and SID-UNN on the proposed RMGD dataset under the four different haze conditions

As shown in Figure 9, I raised the saturation of the hazy input and obtained images in Fig. 9(b). In the selected regions, it is easy to find that a hint of green is on the hazy input and matches exactly with the green regions in the dehazed images. This shade of green usually appears around the shadow in the curtains or the top-right corner, which might result from insufficient lighting and thick haze. It is not a result of colour distortion and incorrectness in the method, but rather, the green colour is initially there in the hazy input, and dehazing strengthens all colours so green pixels appear more obvious.

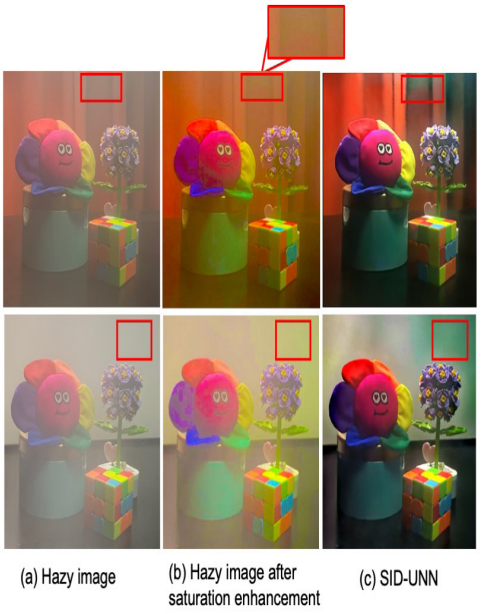

Fig. 9 A visual demonstration of the shade of green present. The selected regions show how the green areas in hazy inputs match those in dehazed images.

5 Conclusion

In this work, a single image dehazing method using an untrained neural network, SID-UNN, has been presented, which uses a nonlinear optimization method to solve a classical ill-posed inverse problem: recover of haze-free image J from input hazy image I. Moreover, the initialization priors, WLS filtering, and smoothing constraints are innovatively introduced to improve the reconstruction rate and maintain high-frequency details in images, promising a clearer perception while effectively diminishing the halo artefacts. Unlike most traditional prior-based SID methods, parameters in estimating transmission maps are optimized iteratively through a network in the proposed methods, thus circumventing the handcrafted adjustments of parameters and reducing the experience dependence. In addition, as is evident from the results, the proposed method can handle images with white backgrounds, a condition that is difficult to deal with using some image priors like DCP. SID-UNN results demonstrate more details, fewer artefacts, and more colour distortions than common prior-based methods. Contrary to many end-to-end deep-learning-based SID methods that are data-driven, SID-UNN does not require massive datasets and pretraining, avoiding the complicated process of procuring massive datasets and image collection and exhibiting better generalization and robustness.

Note that the ideas adopted in the SID-UNN method proposed in this article can be applied to SID problems and to solving other inverse problems. As mentioned in Section 4, shortcomings of my method are not a problem with the SID-UNN method's thinking, but rather limitations with the forward model. In conclusion, the proposed model demonstrates satisfying dehazing ability in synthetic and self-created datasets but faces technological limitations. In the future, by applying SID-UNN to better devices and incorporating better images prior, the model's thinking will bring a larger advantage in real-life dehazing applications.

References

[1] X. Liu, Y. Hui, Z.-Y. Yin, Z. Wang, X. Xie, and J. Fang, 'Deteriorating haze situation and the severe haze episode during December 18–25 of 2013 in Xi'an, China, the worst event on record', *Theor. Appl. Climatol.*, vol. 125, no. 1–2, pp. 321–335, Jul. 2016, doi: 10.1007/s00704-015-1509-8.

[2] R. Balasubramanian, R. Kumar, and B. K. Kaushik, 'FPGA implementation of image dehazing algorithm for real time applications', in *Applications of Digital Image Processing XL*, A. G. Tescher, Ed., San Diego, United States: SPIE, Sep. 2017, p. 111. doi: 10.1117/12.2274682.

[3] K. Gao, H. Tu, L. Sun, N. N. Sze, Z. Song, and H. Shi, 'Impacts of reduced visibility under hazy weather condition on collision risk and car-following behavior: Implications for traffic control and management', *Int. J. Sustain. Transp.*, vol. 14, no. 8, pp. 635–642, Jun. 2020, doi: 10.1080/15568318.2019.1597226.

[4] H. Koschmieder, 'Luftlicht und Sichtweite', *Naturwissenschaften*, vol. 26, no. 32, pp. 521–528, Aug. 1938, doi: 10.1007/BF01774261.

[5] E. J. McCartney, *Optics of the atmosphere: scattering by molecules and particles*. in Wiley series in pure and applied optics. New York: Wiley, 1976.

[6] Kaiming He, Jian Sun, and Xiaoou Tang, 'Single Image Haze Removal Using Dark Channel Prior', *IEEE Trans. Pattern Anal. Mach. Intell.*, vol. 33, no. 12, pp. 2341–2353, Dec. 2011, doi: 10.1109/TPAMI.2010.168.

[7] D. Berman, T. Treibitz, and S. Avidan, 'Single Image Dehazing Using Haze-Lines', *IEEE Trans. Pattern Anal. Mach. Intell.*, vol. 42, no. 3, pp. 720–734, Mar. 2020, doi: 10.1109/TPAMI.2018.2882478.

[8] A. Wang, W. Wang, J. Liu, and N. Gu, 'AIPNet: Image-to-Image Single Image Dehazing With Atmospheric Illumination Prior', *IEEE Trans. Image Process.*, vol. 28, no. 1, pp. 381–393, Jan. 2019, doi: 10.1109/TIP.2018.2868567.

[9] D. Ulyanov, A. Vedaldi, and V. Lempitsky, 'Deep Image Prior', *Int. J. Comput. Vis.*, vol. 128, no. 7, pp. 1867–1888, Jul. 2020, doi: 10.1007/s11263-020-01303-4.

[10] R. Heckel and P. Hand, 'Deep Decoder: Concise Image Representations from Untrained Non-convolutional Networks', Feb. 22, 2019, *arXiv*: arXiv:1810.03982. Accessed: Sep. 07,

ISSN 2959-6157

2024. [Online]. Available: http://arxiv.org/abs/1810.03982

[11] B. Li, Y. Gou, J. Z. Liu, H. Zhu, J. T. Zhou, and X. Peng, 'Zero-Shot Image Dehazing'.

[12] Z. Farbman, R. Fattal, D. Lischinski, and R. Szeliski, 'Edge-preserving decompositions for multi-scale tone and detail manipulation', *ACM Trans. Graph.*, vol. 27, no. 3, pp. 1–10, Aug. 2008, doi: 10.1145/1360612.1360666.

[13] S. Kanti Dhara, M. Roy, D. Sen, and P. Kumar Biswas, 'Color Cast Dependent Image Dehazing via Adaptive Airlight Refinement and Non-Linear Color Balancing', *IEEE Trans. Circuits Syst. Video Technol.*, vol. 31, no. 5, pp. 2076–2081, May 2021, doi: 10.1109/TCSVT.2020.3007850.

[14] B. Li *et al.*, 'Benchmarking Single Image Dehazing and Beyond', Apr. 21, 2019, *arXiv*: arXiv:1712.04143. Accessed: Sep. 13, 2024. [Online]. Available: http://arxiv.org/abs/1712.04143

[15] B. Li, X. Peng, Z. Wang, J. Xu, and D. Feng, 'AOD-Net: All-in-One Dehazing Network', in *2017 IEEE International Conference on Computer Vision (ICCV)*, Venice: IEEE, Oct. 2017, pp. 4780–4788. doi: 10.1109/ICCV.2017.511.

[16] D. Chen *et al.*, 'Gated Context Aggregation Network for Image Dehazing and Deraining', in *2019 IEEE Winter Conference on Applications of Computer Vision (WACV)*, Waikoloa Village, HI, USA: IEEE, Jan. 2019, pp. 1375–1383. doi: 10.1109/WACV.2019.00151.

[17] X. Qin, Z. Wang, Y. Bai, X. Xie, and H. Jia, 'FFA-Net: Feature Fusion Attention Network for Single Image Dehazing', Dec. 05, 2019, *arXiv*: arXiv:1911.07559. Accessed: Sep. 07, 2024. [Online]. Available: http://arxiv.org/abs/1911.07559